Editors' Suggestion

Lateral vesicle migration in a bounded shear flow: Viscosity contrast leads to off-centered solutions

Abdessamad Nait-Ouhra,[1,2,3,*] Achim Guckenberger,[4] Alexander Farutin,[1,2] Hamid Ez-Zahraouy,[3] Abdelilah Benyoussef,[3,5] Stephan Gekle,[4] and Chaouqi Misbah[1,2,†]

[1]*Université Grenoble Alpes, LIPHY, F-38000 Grenoble, France*

[2]*CNRS, LIPHY, F-38000 Grenoble, France*

[3]*Laboratoire de Matière Condensée et Sciences Interdisciplinaires, Faculty of Sciences, Mohammed V University of Rabat, Rabat 1014, Morocco*

[4]*Biofluid Simulation and Modeling, Theoretische Physik VI, Universität Bayreuth, Bayreuth 95440, Germany*

[5]*Hassan II Academy of Science and Technology, Rabat 10220, Morocco*

(Received 2 October 2018; published 5 December 2018)

The lateral migration of a suspended vesicle (a model of red blood cells) in a bounded shear flow is investigated numerically at vanishing Reynolds number (the Stokes limit) using a boundary integral method. We explore, among other parameters, the effect of the viscosity contrast $\lambda = \eta_{\text{in}}/\eta_{\text{out}}$, where η_{in}, η_{out} denote the inner and the outer fluids' viscosities. It is found that a vesicle can either migrate to the center line or towards the wall depending on λ. More precisely, below a critical viscosity contrast λ_c, the terminal position is at the center line, whereas above λ_c, the vesicle can be either centered or off-centered depending on initial conditions. It is found that the equilibrium lateral position of the vesicle exhibits a saddle-node bifurcation as a function of the bifurcation parameter λ. When the shear stress increases the saddle-node bifurcation evolves towards a pitchfork bifurcation. A systematic analysis is first performed in two dimensions (due to numerical efficiency), and the overall picture is confirmed in three dimensions. This study can be exploited in the problem of cell sorting and can help understand the intricate nature of the dynamics and rheology of confined suspensions.

DOI: 10.1103/PhysRevFluids.3.123601

I. INTRODUCTION

The problem of lateral migration (or cross-streamline migration) of small enough particles (where inertia can be neglected) is of considerable importance in many fields, such as in mechanics, physics, chemistry, and biology [1–4]. A particular property of the inertialess limit (or the Stokes limit) is that a rigid particle, when it stays oriented in the shear plane, cannot migrate perpendicularly to the flow direction in a linear shear flow. This is traced back to the invariance of the Stokes equations under time reversal. Soft particles, in contrast, can acquire a cross-streamline migration because their deformation can lead to an upstream-downstream asymmetry, breaking thus the reversibility of the Stokes equations. A particularly studied example of interest to our study is the lift of a vesicle due to a wall [5–20]. This type of lift plays an important role in hemodynamics, where red blood cells (RBCs) have a tendency to accumulate towards the blood vessel center, leaving behind a cell-free layer close to the vessel wall. This effect is accompanied by an ample decrease of blood viscosity [21] upon decreasing the vessel diameter and is commonly known as the Fåhræus-Lindqvist effect [22].

*abdessamad.nait-ouhra@univ-grenoble-alpes.fr

†chaouqi.misbah@univ-grenoble-alpes.fr

When a vesicle is placed in a linear shear flow, i.e., between two parallel planes moving with equal and opposite velocities, it has been reported (in accordance to intuition) that the vesicle will feel symmetric lifts from both walls, so that the ultimate position is a centered one. When the vesicle settles in the center it undergoes a tank-treading motion (provided the viscosity contrast is small enough). For higher viscosity contrast the vesicle may undergo a tumbling dynamics, but the wall-induced lift still operates [23,24] and pushes the vesicle (or RBC) towards the channel center. Indeed, during tumbling, the particle is elongated along its longest axis during one part of the tumbling cycle and compressed during the other one due to the elongational component of the shear flow. This creates an asymmetry of the shape during the two halves of the tumbling period, leading to a net migration (albeit small compared to the case where the vesicle undergoes tank treading).

By investigating systematically the question of a cross-streamline migration in a linear shear flow created by two countertranslating planes, we find that the problem can be more complicated than previously thought. Indeed, the center line does not always correspond to the final position. Instead we find a complex phase diagram, where for low enough viscosity contrast the vesicle always reaches the center, for all sets of initial conditions that we have explored. However, beyond a critical viscosity contrast the vesicle can either reach the center line or move towards one of the two walls and align with the flow. Whether the vesicle chooses one or the other solution depends on initial conditions. In other words, beyond a critical viscosity contrast, there is coexistence of two stable branches of solutions (the centered and the off-centered one). According to the bifurcation theory nomenclature, there should exist a critical viscosity contrast at which the system undergoes a saddle-node bifurcation. This is what will be shown here. Besides the analysis of the bifurcation, we shall also describe the basin of attraction of each solution (when they coexist), as well as the effect of other parameters (reduced area and degree of confinement) on the overall solutions.

When the shear stress increases, it is found that the saddle-node bifurcation evolves into a pitchfork bifurcation. In that case, there is no coexistence, but rather the central position becomes unstable beyond a critical viscosity contrast in favor of an off-centered solution. The first and systematic study is dedicated to a two-dimensional (2D) geometry. Due to computational efficiency, this will allow us to scan a quite large parameter space. At the end, we will devote a brief discussion to the same problem in three dimensions in order to highlight the robust nature of the problem.

In our simulations the viscosity contrast λ is varied in a wide range $\lambda = 1$–50. Experimentally, this range can be achieved with vesicles by adding polymers inside the vesicle (like dextran) [25]. For RBCs, the physiological value of λ is about 5 to 10 [26,27]. In addition, in some blood diseases [28–33], such as sickle cell anemia and malaria, larger values can be achieved.

II. MODEL AND SIMULATION METHOD

A. Membrane model

We consider a vesicle in two or three dimensions immersed in a semi-infinite fluid bounded on the top and bottom by two parallel planes. The vesicle is subjected to a planar shear flow $v_x^0 = \dot{\gamma} y$ (or, in three dimensions, $v_x^0 = \dot{\gamma} z$) with v_x^0 the component along the flow direction of the imposed flow $\mathbf{v}^0$. Here the x axis (x and y in three dimensions) is defined to be parallel to the walls. The vesicle membrane acts on the fluid via bending and tension forces, the latter resulting from membrane inextensibility. The total force in two dimensions is given by [13]

$$\mathbf{f}_{\text{mem}\to\text{flu}} = \kappa \left(\frac{d^2c}{ds^2} + \frac{1}{2}c^3\right)\mathbf{n} - \xi c\mathbf{n} + \frac{d\xi}{ds}\mathbf{t}. \tag{1}$$

An analogous expression in three dimensions can be found, for example, in Ref. [34]. This membrane force per unit area is obtained from the functional derivative of the Helfrich [35,36] bending energy, which reads in two dimensions $E = \frac{\kappa}{2}\int_{\text{mem}} c^2\, ds + \int_{\text{mem}} \xi\, ds$, where κ is the membrane bending rigidity, c is the membrane curvature, s is the curvilinear coordinate along

the membrane, and **n** and **t** are the unit normal and tangent vectors. In addition, ξ is a Lagrange multiplier that enforces membrane inextensibility. The enclosed area A is conserved automatically because of the fluid incompressibility and the membrane impermeability.

B. 2D boundary integral formulation

We consider the limit of vanishing Reynolds numbers (the Stokes limit). The full problem is described by several dimensionless numbers:

$$\lambda = \frac{\eta_{\text{in}}}{\eta_{\text{out}}}, \quad C_\kappa = \frac{\eta_{\text{out}}\dot{\gamma} R_0^3}{\kappa} \equiv \dot{\gamma} t_c, \quad C_n = \frac{2R_0}{W}, \quad \tau = \frac{4\pi A}{L^2}. \tag{2}$$

Here λ is the viscosity contrast with η_{in}, η_{out} denoting the inner and the outer viscosities. C_κ is the capillary number measuring the flow strength over the bending energy of the membrane. In other words, C_κ controls how the shapes of vesicles deform in response to an applied external flow. The timescale t_c is the typical time needed for the vesicle to recover its equilibrium shape after cessation of flow. All times will be measured hereafter in units of t_c. C_n is the degree of confinement, where W is the channel width. τ is reduced area, where L is the vesicle perimeter and the effective radius $R_0 = \sqrt{A/\pi}$.

Because of the linearity of the Stokes equations, we can use the boundary integral method [37] to formulate the dynamics of the vesicle. For a point $\mathbf{r}_0$ which belongs to a membrane, the velocity $\mathbf{v}(\mathbf{r}_0)$ of this point has the following dimensionless expression in two dimensions:

$$\begin{aligned}\mathbf{v}(\mathbf{r}_0) = {} & \frac{2}{1+\lambda}\mathbf{v}^0(\mathbf{r}_0) + \frac{1}{2\pi C_\kappa (1+\lambda)} \int_{\text{mem}} ds\, \mathbf{f}_{\text{mem}\to\text{flu}}(\mathbf{r}) \cdot \mathsf{G}^{2w}(\mathbf{r}, \mathbf{r}_0) \\ & + \frac{1-\lambda}{2\pi(1+\lambda)} \int_{\text{mem}} ds\, \mathbf{v}(\mathbf{r}) \cdot \mathsf{T}^{2w}(\mathbf{r}, \mathbf{r}_0) \cdot \mathbf{n}(\mathbf{r}),\end{aligned} \tag{3}$$

where we have used the following scales: $R_0 = \sqrt{A/\pi}$ for the length, $U = \dot{\gamma} R_0$ for the velocity, and κ/R_0^3 for the force per unit area. $\mathsf{G}^{2w}(\mathbf{r}, \mathbf{r}_0)$ and $\mathsf{T}^{2w}(\mathbf{r}, \mathbf{r}_0)$ are the Green's functions (second- and third-order tensors) satisfying the no-slip boundary condition at the bounding walls (see Refs. [38,39] for more details). The dimensionless force $\mathbf{f}_{\text{mem}\to\text{flu}}$ is given formally by the same expression in Eq. (1) in which membrane bending rigidity κ is set to unity (we keep the same notation for simplicity).

The still unknown Lagrange multiplier ξ is obtained by imposing a divergence-free velocity along the membrane, expressing the membrane incompressibility. The numerical method of imposing membrane incompressibility follows closely that presented in Ref. [40].

The displacement in the course of time of the vesicle membranes is obtained by updating the discretization points after each time step using an Euler scheme $\mathbf{r}_0(t + dt) = \mathbf{v}(t)dt + \mathbf{r}_0(t)$.

C. 3D boundary integral formulation

For the three-dimensional (3D) simulation we consider, as for the 2D case, the limit of vanishing Reynolds numbers and use the 3D periodic boundary integral method as described in Ref. [41] and validated in Refs. [14,42,43]. The setup employs a single oblate vesicle with a viscosity contrast of λ placed between two parallel walls. Exploiting the translational invariance, the vesicle is fixed in the x and y directions (parallel to the walls) but can move freely in the z direction (perpendicular to the walls). Even in three dimensions, a vesicle does not exhibit any shear elasticity. We model the vesicle's bending rigidity according to the Helfrich model with a bending modulus κ [35,36]. The force (per unit area) $\mathbf{f}_{\text{mem}\to\text{flu}}$ can be expressed as

$$\mathbf{f}_{\text{mem}\to\text{flu}} = 2\kappa[2c(c^2 - K) + \Delta^s c]\mathbf{n}. \tag{4}$$

Here c is the mean curvature, K the Gaussian curvature, and Δ^s the Laplace-Beltrami operator. Numerically, we compute the surface force via the parabolic fitting method from Ref. [44] (a detailed

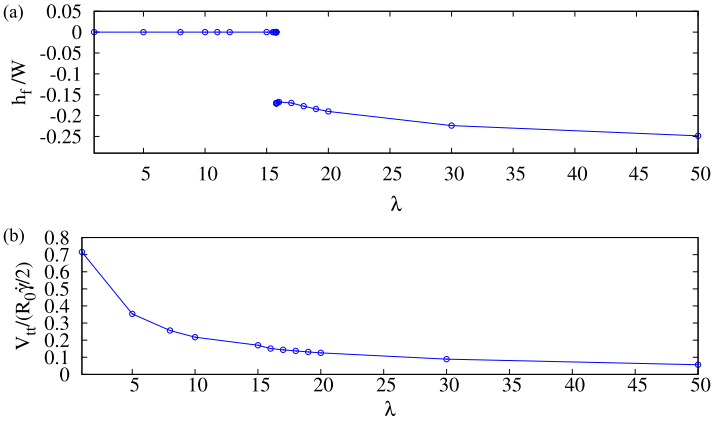

FIG. 1. The evolution of the equilibrium lateral position h_f and the dimensionless tank treading velocity $V_{tt}/(R_0\dot{\gamma}/2)$ (a and b, respectively) according to the bifurcation parameter λ. Here $\tau = 0.7$, $C_\kappa = 1$, and $W/R_0 = 5$. $R_0\dot{\gamma}/2$ is the velocity of membrane of a circular vesicle under shear flow in unbounded geometry.

analysis can be found in Ref. [45]; see Method E therein). The spontaneous curvature is set to zero. An artificial volume drift of the vesicle is countered by employing the no-flux condition and the rescaling method as in Ref. [41]; i.e., the volume V is perfectly conserved. The global surface area is kept approximately constant via an effective surface force with a surface modulus of $\kappa_A = 2000\kappa/R_0^2$. This results in typical surface deviations of $\lesssim 0.3\%$, which is consistent with Ref. [34]. The mesh is stabilized by employing the procedure from Ref. [41, Eq. (2.74)] (which is very similar to Ref. [44, Eq. (59)]) with a strength of $\zeta = 0.03$ (ζ is a parameter that controls the stiffness of the scheme used the prevent the large distortions of the mesh). The surface is discretized with 1280 flat triangles.

The full 3D problem is described by the same dimensionless numbers as the previous 2D case, with a slight difference for the reduced volume, which is given by $\tau^{3D} = 6\sqrt{\pi}V/A'^{3/2}$ (with the vesicle volume V and surface area A') and an effective radius defined as $R_0 = [3V/(4\pi)]^{1/3}$.

Numerically, the boundary integral equation is computed with seven Gauss points per triangle and appropriate singularity removal [41]. The calculation of the periodic Green's functions is accelerated with the SPME method [46] with cutoff errors below 10^{-4}. GMRES is used to solve the linear system with a target residual of 10^{-4}. Time integration is performed via the adaptive Bogacki-Shampine method with the absolute tolerance set to $10^{-5}R_0$ and the relative tolerance set to 10^{-5}.

III. RESULTS

A. Off-centered stable positions beyond a critical viscosity contrast

We first start by describing systematically the results for the 2D model. The 3D simulations show a qualitatively similar behavior, as shown in the last subsection. In this section we investigate the influence of the viscosity contrast λ on the equilibrium lateral position of the vesicle. The lateral migration of a vesicle is described using the vesicle's center of mass. Initially the vesicle is located at a small enough distance ($0.72R_0$) from the lower wall and is then subjected to a shear flow. Figure 1 contains the first central result, showing the final position h_f (distance from the center of the channel to the center of mass of the vesicle) as a function of λ. Here the other parameters are kept fixed: $\tau = 0.7$, $C_\kappa = 1$, and $W/R_0 = 5$. As shown in that figure, below a critical value of λ ($\lambda_c \simeq 16$) the final position corresponds to the center of the channel; note that the center line is at 0 on the vertical axis in Fig. 1(a) and the lower wall is at -0.5. In this case (centered vesicle), the vesicle dynamics correspond to the classical behavior [27,39,40,47–49]: tank-treading motion (TT)

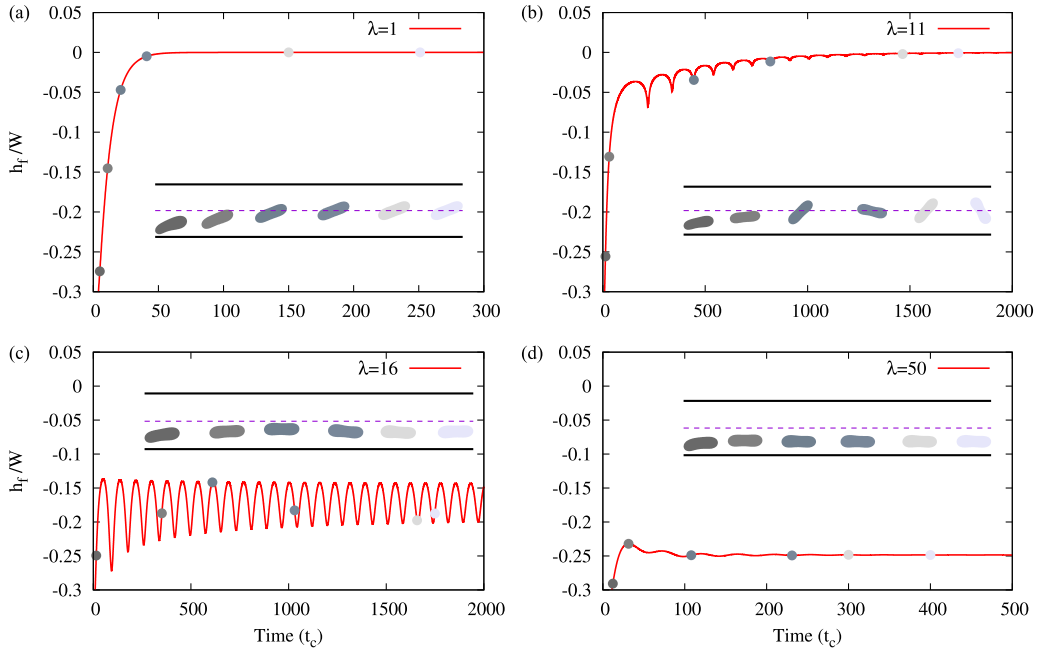

FIG. 2. The evolution of the lateral position of the vesicle h_f as a function of time (in units of t_c) for several λ. The center is at 0 on the vertical axis, and the lower wall is at -0.5. In this case, below $\lambda_c = 16$, the vesicle is centered. For very low λ (TT motion), it reaches the center of the channel faster, while for larger lambda, but still below λ_c, TB motion is observed, and the time to reach the center becomes significantly longer. Beyond λ_c the vesicle is off-centered. A typical sequence of snapshots are shown. Here we set $C_\kappa = 1$, $\tau = 0.7$ and $W/R_0 = 5$. We note that in panel (c) ($\lambda = 16$), the final value of h_f is computed as a time average over more than $4000t_c$.

when λ is small enough ($\lambda \lesssim 10$) and tumbling regime (TB) for $\lambda \gtrsim 10$. In both cases the vesicle feels a wall-induced lift that pushes it towards the center line. However, the vesicle in the TT regime ($\lambda = 1$, Fig. 2) reaches the center line faster than in the case of TB motion ($\lambda = 11$). Figures 2(a) and 2(b) show the behavior in the course of time in the case where the vesicle undergoes TT and TB, respectively.

An interesting feature is discovered for higher values of λ. Indeed, for $\lambda \gtrsim \lambda_c$, the vesicle, initially located close to the wall, lifts off slightly and never reaches the center line. Instead, it tends with time to a final off-centered position [Figs. 2(c) and 2(d)]. In addition, the vesicle, despite high values (up to 50) of the viscosity contrast, never showed TB and rather exhibits a flow alignment (FA), where the vesicle is off-centered and almost aligned with the flow (vesicle's long axis is parallel to the flow direction) while the membrane performs TT with a lower tank-treading velocity (V_{tt}) than that of the TT and TB motions [Fig. 1(b)].

Note that above the critical value of viscosity contrast λ_c but close to it, the vesicle reaches its final off-centered position in a nonmonotonous way with time, by undergoing quite ample oscillations [Fig. 2(c)]. Note, finally, that when $\lambda > \lambda_c$ the vesicle always reaches an off-centered position. We will see later that the situation is more complex, since the final position is sensitive to initial position (see Sec. III C).

In the following section we investigate the effect of the channel width on the dynamics of the vesicle, and we shall provide some intuitive mechanisms controlling the equilibrium lateral position of the vesicle within the channel.

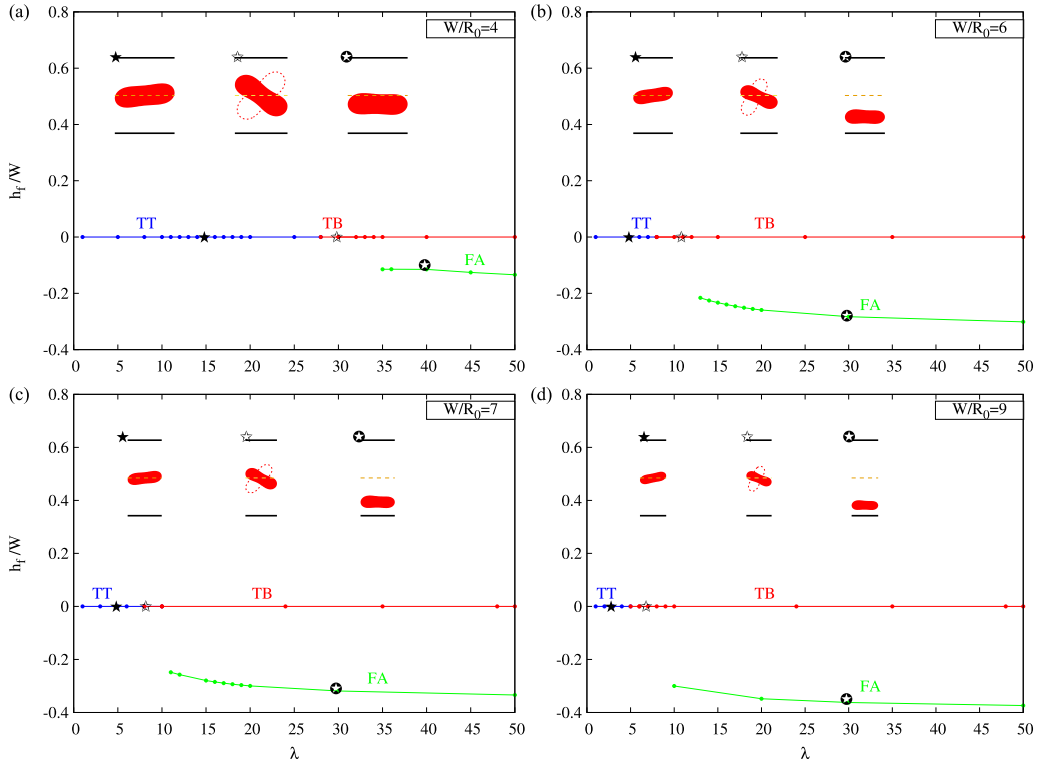

FIG. 3. The evolution of the equilibrium lateral position h_f as a function of the bifurcation parameter λ for several channel width W. Here we set $C_\kappa = 1$ and $\tau = 0.7$ and the initial position of the vesicle is close enough to the lower wall. Beyond λ_c the vesicle is initially set either at the center or at a small enough distance $(0.72R_0)$ from the lower wall. TT, TB, and FA are shown.

B. Effect of channel width and qualitative physical arguments for the emergence of the off-centered solution

We have analyzed the role played by the confinement (see Fig. 3) by considering an initial position close enough to the lower wall. The three main regimes attained by a vesicle in shear flow for $W/R_0 = 5$, TT, TB, and FA (see the previous section), persist for all explored values of confinement. Each value of W (Fig. 3) is associated with a critical viscosity contrast $\lambda_c(W)$, below which the particle always migrates away from the wall to the center line of the channel, whereas beyond $\lambda_c(W)$ an off-centered position with FA is attained by the vesicle.

A high confinement favors the centered solution, as can be seen in Figs. 3 and 4. This result is quite intuitive. In short, the main effect of the confinement is to shift the transition threshold value λ_c to higher values upon increasing the degree of confinement.

Let us now provide some mechanisms controlling the stable lateral position. Our results (Fig. 3) show that below λ_c the vesicle can either perform a TT motion or a TB motion. In the pure TT regime the wall-induced lift is so strong that the vesicle continues to migrate until it reaches the center where the effects of the two walls compensate each other. Upon increasing λ the vesicle undergoes a TB transition. A linear shear flow can be viewed as a superposition of a rotational and an elongational flow [Fig. 5(a)]. If λ is not too large the TB vesicle still shows some deformation, and during one half of the TB cycle, the vesicle is oriented with its long axis having positive angle with the horizontal axis, in which case it is elongated by the shear flow and will lift off with a certain amplitude. During the second half of the TB cycle the vesicle long axis is oriented along negative

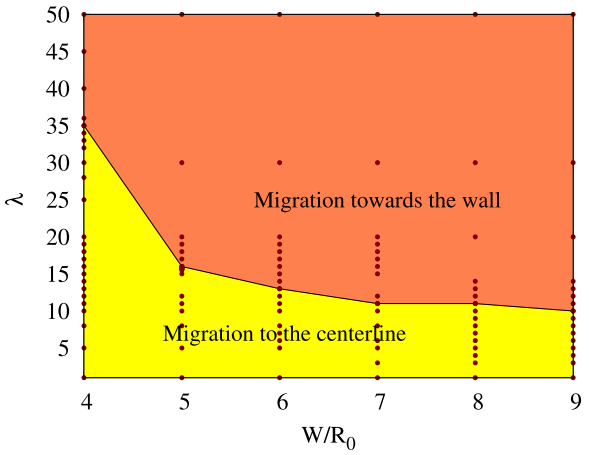

FIG. 4. Phase diagram showing regions where migration is towards the center or towards the wall depending on λ and W. Migration towards the center line is favored by confinement (small W). The solid line is a guide for the eyes. The simulations data are shown as dots. Here we set $\tau = 0.7$ and $C_\kappa = 1$.

angles, and it is compressed by the shear flow. Thus its migration speed is lower than in the first half of the cycle. Thus, globally the vesicle will lift off, albeit less than in the TT regime, and finally reaches the center.

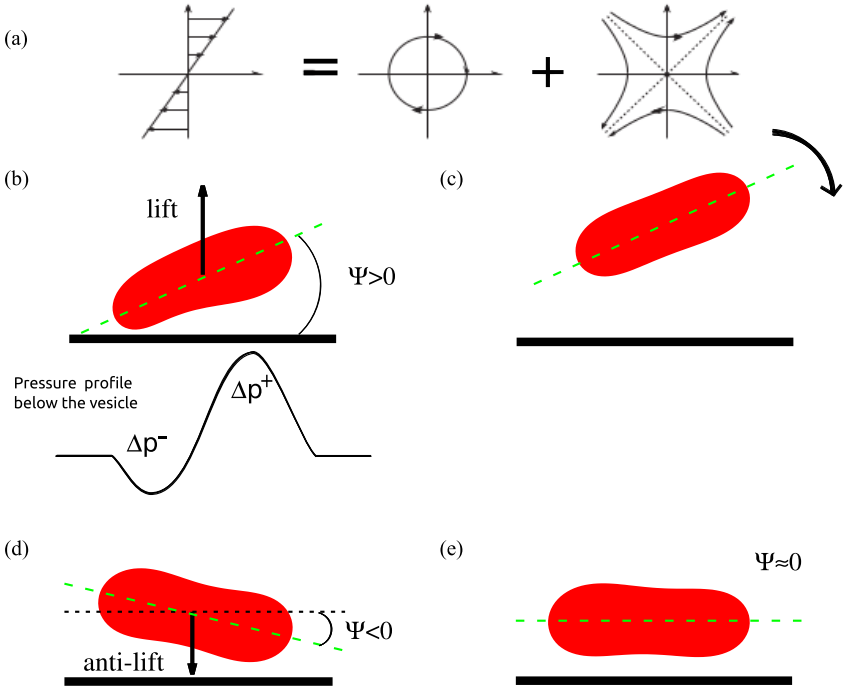

FIG. 5. (a) Decomposition of the linear shear flow into pure rotational and elongational components. (b)–(e) Schema showing the link between the orientation angle of the vesicle with the direction of the flow (horizontal axis) and the lift of the vesicle. We show here the pressure profile given in Ref. [8] as an illustration.

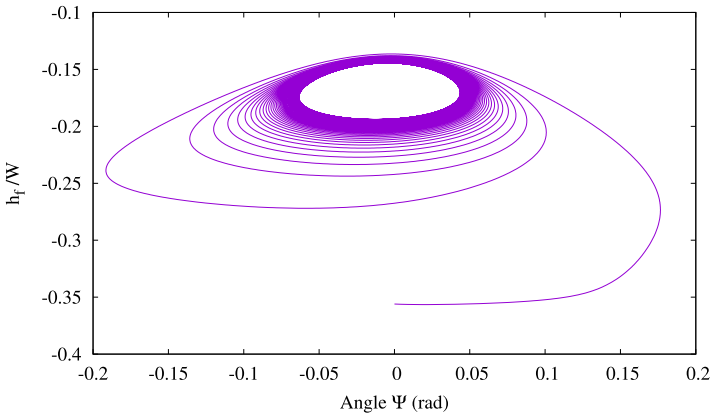

FIG. 6. Angle Ψ vs lateral position of the vesicle h_f. Here $\lambda = 16$, $C_\kappa = 1$, and $W = 5R_0$.

In the vicinity of λ_c, the vesicle still has a small tendency to lift off [Fig. 5(b)] due to a small upstream or downstream asymmetry, and may acquire a slightly positive angle [Fig. 5(c)] [6,8,10]. Since the viscosity contrast is large enough, the vesicle, once it has started lifting, will be subject to TB, which has an antagonist effect, causing the lift-off angle to decrease, and even to reverse it [TB is clockwise; Fig. 5(d)]. The vesicle will then have an antilift pushing it back towards the wall. Once close to the wall, the vesicle aligns with the wall. At the wall [Fig. 5(e)] due to an overpressure ahead and underpressure at the rear [6,8,10] the lubrication forces causing lift become again strong enough to lift off the vesicle, which again faces the antagonist effect of TB, and so on. The interplay of these two antagonist effects leads to an oscillation of the vesicle position (as seen in Fig. 2). When λ is increased further and further the TB effect always wins and acts to stick the vesicle close to the wall and force it to align with the wall, leading to a permanent flow alignment.

In short, from Fig. 6 we see that the migration away from the walls is associated with a positive orientation angle, whereas the opposite happens for a negative tilt angle. Ultimately the vesicle settles at a certain y position where it is almost aligned with the flow direction ($\Psi \simeq 0$).

C. Effect of the initial position

We will now dig further into the existence of different branches of solutions. For that purpose, we investigate how the initial position of the vesicle affects its final stable position by performing a systematic study varying the initial position of the vesicle within a channel for different values of λ. We set $W = 5R_0$, $C_\kappa = 1$, and $\tau = 0.7$.

In Fig. 7 we find that the initial position does not affect the final position of the vesicle if $\lambda \lesssim \lambda_c$. For all initial positions explored in the simulations, the vesicle is found to migrate towards the center line independent of the initial position. In other words, the basin of attraction of this solution seems to be the whole channel width. The situation is different for $\lambda \gtrsim \lambda_c$. The vesicle can either migrate towards the wall or towards the center line of the channel. It migrates towards the wall if its initial position is within the orange area (the basin of attraction) and towards the center line if its initial position is within the yellow area (the basin of attraction of this solution) in Fig. 7. The blue curve in Fig. 7 corresponds to the final stable position of the vesicle if its initial position is within the orange area. Even when the initial position of the vesicle is above the solid blue curve but within the orange area (between the solid and dashed blue line), the vesicle is attracted towards the blue solid line, which is thus a stable branch.

In order to check the stability of this branch, we introduce a small perturbation of the equilibrium lateral position of the vesicle for a specific value of λ as shown in Fig. 8. After a few characteristic times, the center of mass of the vesicle comes back to its equilibrium position, meaning the (linear)

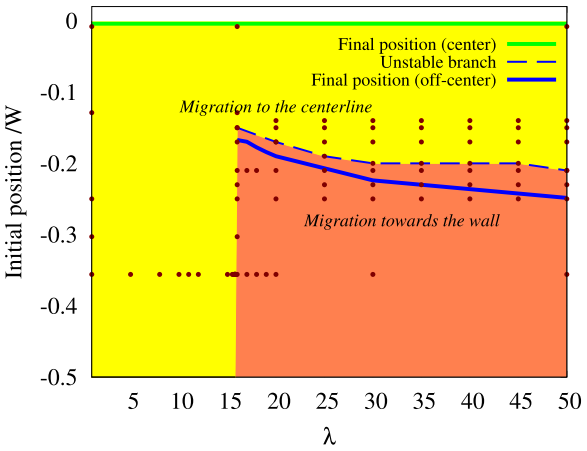

FIG. 7. Phase diagram showing regions where migration is towards the center (if initial position is within yellow area) or towards the wall (if initial position is within orange area). The saddle-node bifurcation occurs at $\lambda_c \simeq 16$ for a reduced area $\tau = 0.7$, a capillary number $C_\kappa = 1$, and a channel width $W = 5R_0$. The channel center is at zero, and the wall is at -0.5 on the vertical axis. The simulations data are shown as dots.

stability of the solution. If we set initially the vesicle in the vicinity of the dashed blue curve, but in the yellow region, the vesicle migrates towards the center line for each value of λ. Thus the solid blue line is a stable branch, whereas the dashed blue line is unstable. The two stable lines (solid blue and solid green lines) are thus separated by the unstable (blue dashed line) branch. This is a typical situation of coexistence of solutions. The solid blue line is a node (in the language of dynamical systems), and the dashed line is a saddle. Thus, in principle the solid and dashed blue lines should intersect on the left side in Fig. 7 (around $\lambda \sim 16$ with a vertical tangent), corresponding to a saddle-node bifurcation point [50]. However, it was not easy to detect this point with a good enough precision, as there is a discontinuous jump close to the saddle-node point. We have seen that the final position of the vesicle is affected by its initial position if $\lambda \geqslant \lambda_c$.

Besides varying the initial position, we also run simulations for vesicles with the same position but different orientations. We observe that indeed the initial orientation of the vesicle can also affect its final position, i.e., whether the vesicle chooses one of the two steady branches depends on orientation.

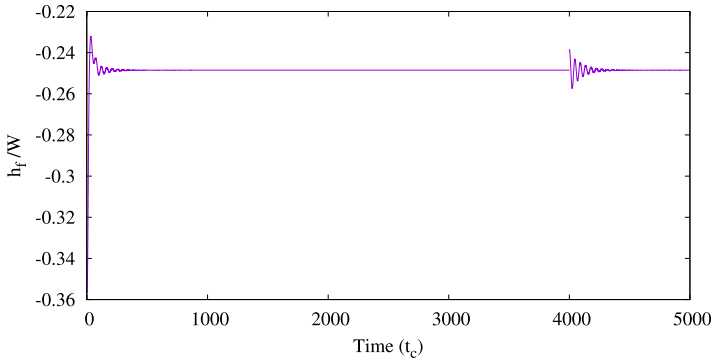

FIG. 8. Lateral position of the vesicle h_f vs time before and after a small destabilization. From this figure we see clearly that the final solution (i.e., final position) is stable. Here $\lambda = 50$, $C_\kappa = 1$, $W = 5R_0$, and $\tau = 0.7$.

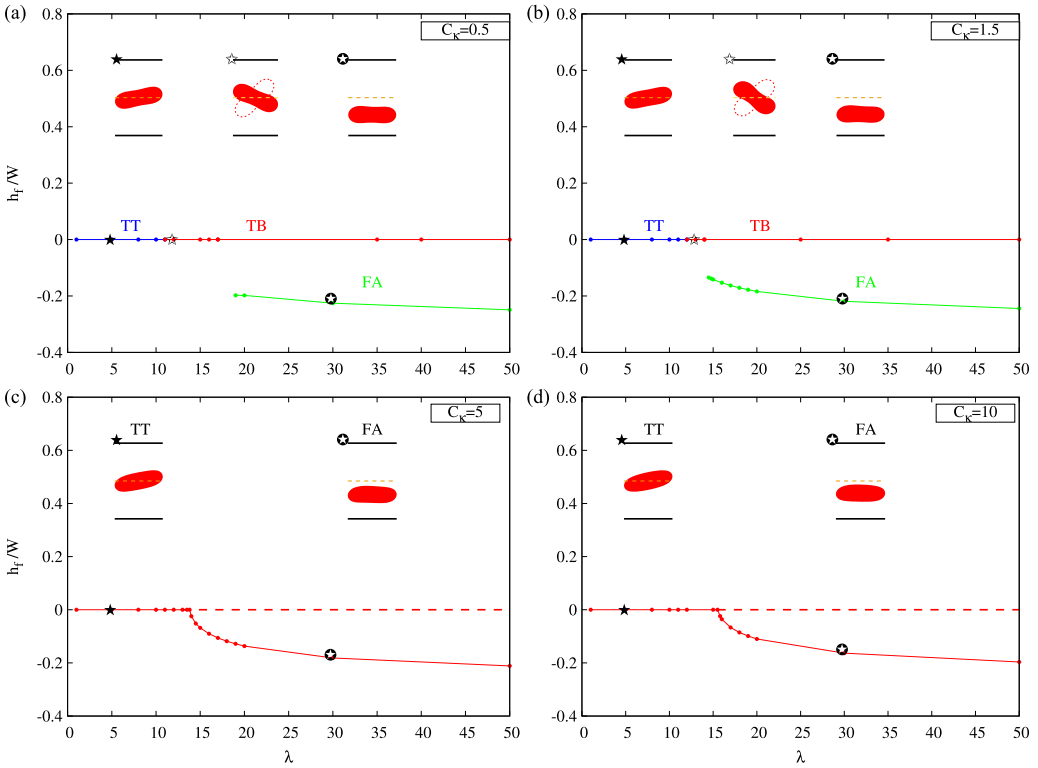

FIG. 9. The evolution of the equilibrium lateral position h_f according the bifurcation parameter λ for several capillary numbers C_κ. The initial position of the vesicle is close enough to the lower wall. Beyond λ_c the vesicle is initially set at the center line or at a small enough distance ($0.72R_0$) from the lower wall. TT, TB, and FA are shown. Beyond a certain value of C_κ, the TB motion is suppressed.

D. Effect of capillary number

In this section we investigate the effect of capillary number C_κ (this parameter controls the deformability of the vesicle under flow). Capillary numbers $C_\kappa \gg 1$ imply large flow rates and thus in general large deformation. The other parameters are kept fixed: $W = 5R_0$, $\tau = 0.7$, and we set the vesicle initially close enough to the lower wall. Here our aim is not to study sensitivity to initial conditions, but rather to analyze the evolution of the new off-centered solution. This is why the initial position is set close to the wall. The explored capillary number range is 0.5–10. Figure 9 illustrates the effect of C_κ on the equilibrium lateral position of the vesicle within the channel. The main difference with previous results is that upon increasing C_κ the line representing the final position as a function of λ exhibits less and less stronger jumps at the bifurcation point. Our results show even that above a certain value of C_κ ($C_\kappa \gtrsim 2.5$), the equilibrium lateral position of the vesicle h_f does not undergo any discontinuity as a function of λ. In other words, we have an evolution from a saddle-node bifurcation into a pitchfork one. To further support this conclusion, we have run simulations for $\lambda > \lambda_c$ by setting the vesicle in the center line. After some time, due to numerical noise, the vesicle left the center towards an off-centered final position, meaning that (unlike the case where C_κ is small) the central position is linearly unstable. It is interesting to note that the change of the nature of the bifurcation (from saddle-node to pitchfork) seems to coincide with the disappearance of the TB motion. More precisely, upon increasing the viscosity contrast λ the vesicle shows TT motion with central position, and at a critical λ, its equilibrium position gradually moves from the center towards the wall (by still performing TT). When λ is far enough

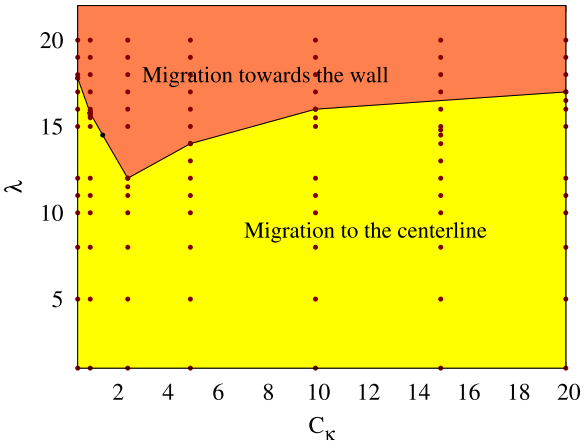

FIG. 10. Phase diagram showing regions where migration is towards the center or towards the wall depending on λ and C_κ. We see here that the capillary number (C_κ) has a nonmonotonic effect on the lateral position of the vesicle; see the text for explanation. The solid line is a guide for the eye. The simulations are shown as dots. Here we set $\tau = 0.7$ and $W = 5R_0$. Initially the vesicle is close enough to the one of the walls.

from the critical value, the vesicle shows a flow alignment. Note that the absence of TB by increasing λ is favored by the presence of the bounding walls. It is known in an unbounded linear shear flow in three dimensions that if the vesicle is in the TB regime, then an increase of C_κ suppresses TB in favor of vacillating breathing or even flow alignment [34,49,51–53]. The phase diagram in Fig. 10 shows the regions where the vesicle migrates towards the center and those where it migrates towards the wall (by having an initial position close to the wall). The widening of the basin of attraction of the central position beyond $C_\kappa \simeq 2.5$ is attributed to the ample increase of deformability that favors the wall induced migration.

E. Effect of reduced area

Finally, let us give a brief report on the influence of the reduced area τ (for a circle $\tau = 1$, otherwise $\tau < 1$). The results are shown in Fig. 11. The other parameters are fixed as $W = 5R_0$ and $C_\kappa = 1$. The vesicle is set initially at a small distance from the lower wall. The range of viscosity contrast over which the TB motion survives (with, as before, migration towards the center) becomes wider with τ. This means that the transition towards FA is delayed. This is shown by the widening of the yellow region in Fig. 12. When τ increases the vesicle becomes more and more rounded (i.e., less elongated) so that the TB strength becomes weaker to force the vesicle to align with the wall in the vicinity of the wall. The vesicle migration towards the center wins over the antagonist TB effect (see Fig. 5, which explains competition between TB and lift off).

F. 3D results

The question naturally arises whether the above 2D results are a consequence of dimensionality or whether they point to a more general phenomenon. To indicate that the observed phenomena are not an artifact of the 2D model, we here devote a brief discussion to the 3D case thus validating the key results of the 2D studies. The details of the numerical procedure can be found in Ref. [41] and in the Methods section of this work. We have set the reduced volume $\tau^{3D} = 0.7$, the channel width $W = 5R_0$, and the capillary number $C_\kappa = 1$. For each value of λ, we start with the vesicle at different initial z positions: In the center ($z_0 = 0$) and off-centered at $z_0/R_0 = \pm 1.2$, except for $\lambda > 40$, where we use $z_0/R_0 = \pm 1$ for stability reasons. We then consider the average z position in the steady state, which we denote as h_f as in the 2D case. The result can be seen in Fig. 13. For small

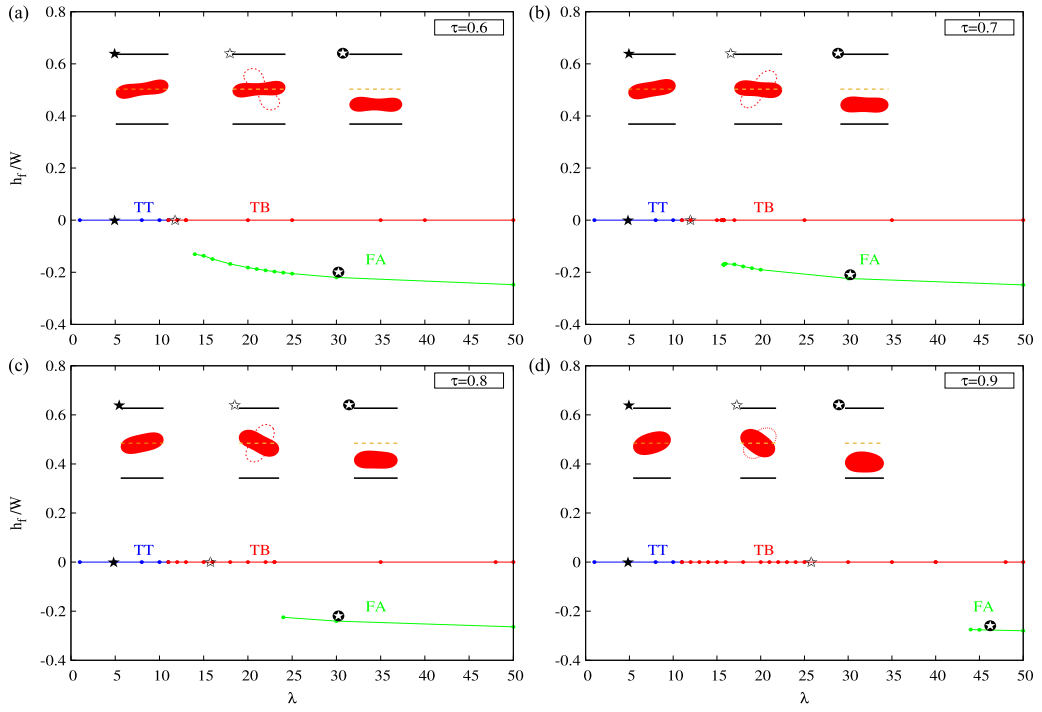

FIG. 11. The evolution of the equilibrium lateral position h_f according to the bifurcation parameter λ for several reduced area τ. Here we set $C_\kappa = 1$ and $W = 5R_0$. Initially the vesicle is close enough to one of the walls. Beyond λ_c the vesicle is initially set at the center line or at a small enough distance ($0.72R_0$) from the lower wall. TT, TB, and FA are shown.

values of λ, the vesicle always moves towards the center ($h_f \approx 0$), in good qualitative agreement with the previous 2D results. However, above a critical threshold of $\lambda \approx 25$, the vesicle assumes an off-centered position near the walls ($h_f \neq 0$). The slight asymmetry for the two off-center starting

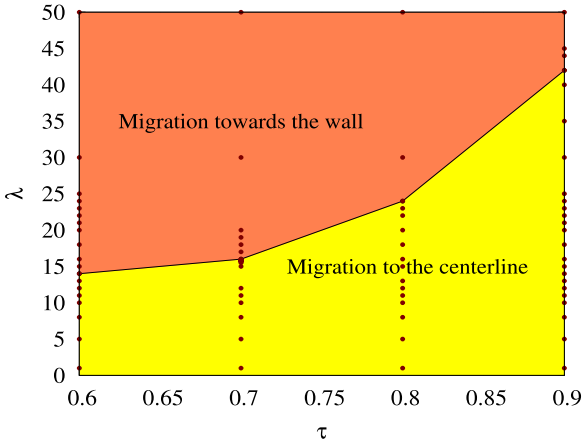

FIG. 12. Phase diagram showing regions where migration is towards the center or towards the wall depending on λ_c and reduced area τ. Migration towards the center line is favored with increasing τ. The solid line is a guide for the eyes. The simulations data are shown as dots. Here we set $W = 5R_0$ and $C_\kappa = 1$.

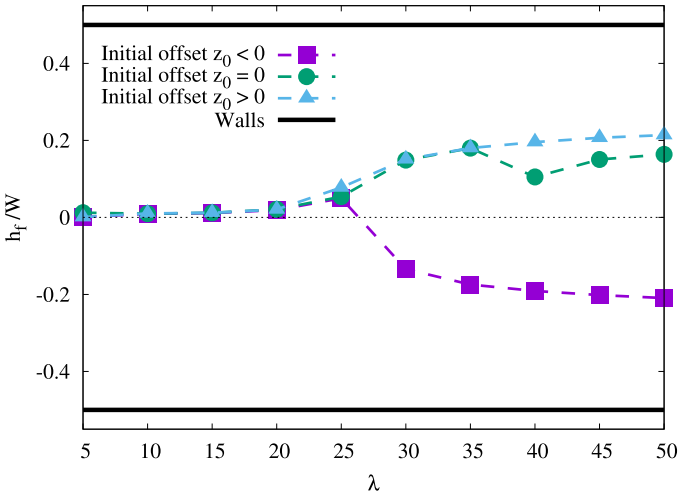

FIG. 13. Average steady-state z position h_f for a 3D vesicle as a function of the viscosity ratio λ. Three different initial positions are used: in the center ($z_0 = 0$) and near the walls ($z_0 \lessgtr 0$). Here we set $W = 5R_0$, $\tau^{3D} = 0.7$, and $C_\kappa = 1$.

positions at $\lambda = 25$ is a numerical artifact, stemming from the fact that we need to solve a Fredholm equation of the mixed kind. In most cases, the vesicle tumbles. Exceptions are found only at $\lambda = 5$, where the vesicle assumes a tank-treading dumbbell shape when started off-centered, and at $\lambda \geqslant 40$, where the vesicle exhibits a rolling motion when started in the center. The latter also explains why the $z_0 = 0$ branch in Fig. 13 is distinct for $\lambda \geqslant 40$.

In short, we confirm in three dimensions that the vesicle under linear shear flow migrates towards the center for lower values of λ and towards the wall for values of λ above a critical value. These results are qualitatively consistent with the 2D results. Note that the presence of a third dimension can allow the vesicle to undergo different kinds of out-of plane motion, which may make the phase diagram quite complex. We hope to report on this matter in the future.

IV. CONCLUSION

In this article, the dynamical behavior of a single vesicle in a confined shear flow as a function of viscosity contrast λ has been investigated numerically. We have performed a systematic study in two dimensions on the effect of the relevant parameters: capillary number (C_κ), channel width (W), and reduced area (τ) on the equilibrium lateral position of the vesicle. We have seen that below a critical viscosity contrast λ_c, the ultimate position of the vesicle is at the center line, whereas above λ_c, the vesicle can be either centered or off-centered depending on initial conditions. Finally, we carried out a 3D numerical simulation to confirm the overall picture obtained in two dimensions.

The revelation here of the existence of different kinds of solutions may lead to different suspension structuring when the concentration is increased. This structuring is expected to impact the rheological properties of the suspension. This constitutes the next interesting step. Finally, the dependence of solutions on the viscosity contrast as well as on the capillary number offers a versatile potential to manipulate and sort deformable particles depending on their internal viscosity and their compliance.

ACKNOWLEDGMENTS

We thank CNES (Centre National d'Etudes Spatiales), ESA (European Space Agency), the French-German university programme "Living Fluids" (grant CFDA-Q1-14), and the German

Research Foundation (DFG) within the collaborative research center TRR225 (subproject B07). A.N.-O. would to thank CNRST Morocco for awarding a scholarship of excellence (Grant Ref. k 1/045). The simulations were performed on the Cactus cluster of the CIMENT infrastructure, which is supported by the Rhône-Alpes region (Grant CPER07_13 CIRA) and on the SuperMUC system operated by the Leibniz Rechenzentrum in Garching.

[1] R. G. Larson, *The Structure and Rheology of Complex Fluids* (Oxford University Press, New York, 1999), Vol. 33.
[2] P.-G. De Gennes and P.-G. Gennes, *Scaling Concepts in Polymer Physics* (Cornell University Press, Ithaca, NY, 1979).
[3] M. Doi and S. F. Edwards, *The Theory of Polymer Dynamics* (Oxford University Press, New York, 1988), Vol. 73.
[4] Y.-C. Fung, *Biomechanics: Circulation* (Springer Science & Business Media, New York, 2013).
[5] U. Seifert, Hydrodynamic Lift on Bound Vesicles, Phys. Rev. Lett. **83**, 876 (1999).
[6] S. Sukumaran and U. Seifert, Influence of shear flow on vesicles near a wall: A numerical study, Phys. Rev. E **64**, 011916 (2001).
[7] P. Olla, The behavior of closed inextensible membranes in linear and quadratic shear flows, Physica A **278**, 87 (2000).
[8] I. Cantat and C. Misbah, Lift Force and Dynamical Unbinding of Adhering Vesicles Under Shear Flow, Phys. Rev. Lett. **83**, 880 (1999).
[9] P. Olla, The lift on a tank-treading ellipsoidal cell in a shear flow, J. Phys. II France **7**, 1533 (1997).
[10] P. Olla, The role of tank-treading motions in the transverse migration of a spheroidal vesicle in a shear flow, J. Phys. A **30**, 317 (1997).
[11] P. Olla, Simplified Model for Red Cell Dynamics in Small Blood Vessels, Phys. Rev. Lett. **82**, 453 (1999).
[12] G. Coupier, B. Kaoui, T. Podgorski, and C. Misbah, Noninertial lateral migration of vesicles in bounded Poiseuille flow, Phys. Fluids **20**, 111702 (2008).
[13] B. Kaoui, G. H. Ristow, I. Cantat, C. Misbah, and W. Zimmermann, Lateral migration of a 2D vesicle in unbounded Poiseuille flow, Phys. Rev. E **77**, 021903 (2008).
[14] A. Guckenberger, A. Kihm, T. John, C. Wagner, and S. Gekle, Numerical–experimental observation of shape bistability of red blood cells flowing in a microchannel, Soft Matter **14**, 2032 (2018).
[15] M. Abkarian and A. Viallat, Vesicles and red blood cells in shear flow, Soft Matter **4**, 653 (2008).
[16] D. S. Hariprasad and T. W. Secomb, Prediction of noninertial focusing of red blood cells in Poiseuille flow, Phys. Rev. E **92**, 033008 (2015).
[17] Q. M. Qi and E. S. G. Shaqfeh, Theory to predict particle migration and margination in the pressure-driven channel flow of blood, Phys. Rev. Fluids **2**, 093102 (2017).
[18] Q. M. Qi and E. S. G. Shaqfeh, Time-dependent particle migration and margination in the pressure-driven channel flow of blood, Phys. Rev. Fluids **3**, 034302 (2018).
[19] B. Kaoui, G. Biros, and C. Misbah, Why Do Red Blood Cells Have Asymmetric Shapes Even in a Symmetric Flow? Phys. Rev. Lett. **103**, 188101 (2009).
[20] J. Beaucourt, T. Biben, and C. Misbah, Optimal lift force on vesicles near a compressible substrate, Europhys. Lett. **67**, 676 (2004).
[21] A. Pries, D. Neuhaus, and P. Gaehtgens, Blood viscosity in tube flow: dependence on diameter and hematocrit, Am. J. Physiol. Heart Circ. Physiol. **263**, H1770 (1992).
[22] R. Fåhræus and T. Lindqvist, The viscosity of the blood in narrow capillary tubes, Am. J. Physiol. **96**, 562 (1931).
[23] X. Grandchamp, G. Coupier, A. Srivastav, C. Minetti, and T. Podgorski, Lift and Down-Gradient Shear-Induced Diffusion in Red Blood Cell Suspensions, Phys. Rev. Lett. **110**, 108101 (2013).
[24] Z. Shen, A. Farutin, M. Thiébaud, and C. Misbah, Interaction and rheology of vesicle suspensions in confined shear flow, Phys. Rev. Fluids **2**, 103101 (2017).

[25] M.-A. Mader, C. Misbah, and T. Podgorski, Dynamics and rheology of vesicles in a shear flow under gravity and microgravity, Microgravity Sci. Technol. **18**, 200 (2006).
[26] A. M. Forsyth, J. Wan, P. D. Owrutsky, M. Abkarian, and H. A Stone, Multiscale approach to link red blood cell dynamics, shear viscosity, and ATP release, Proc. Natl. Acad. Sci. USA **108**, 10986 (2011).
[27] V. Vitkova, M.-A. Mader, B. Polack, C. Misbah, and T. Podgorski, Micro-macro link in rheology of erythrocyte and vesicle suspensions, Biophys. J. **95**, L33 (2008).
[28] S. Chien, S. Usami, and J. F. Bertles, Abnormal rheology of oxygenated blood in sickle cell anemia, J. Clin. Invest. **49**, 623 (1970).
[29] Y. Imai, H. Kondo, T. Ishikawa, C. T. Lim, and T. Yamaguchi, Modeling of hemodynamics arising from malaria infection, J. Biomech. **43**, 1386 (2010).
[30] H. Bow, I. V. Pivkin, M. Diez-Silva, S. J. Goldfless, M. Dao, J. C. Niles, S. Suresh, and J. Han, A microfabricated deformability-based flow cytometer with application to malaria, Lab Chip **11**, 1065 (2011).
[31] S. Suresh, Mechanical response of human red blood cells in health and disease: Some structure-property-function relationships, J. Mater. Res. **21**, 1871 (2006).
[32] G. A. Barabino, M. O. Platt, and D. K. Kaul, Sickle cell biomechanics, Annu. Rev. Biomed. Eng. **12**, 345 (2010).
[33] X. Li, P. M. Vlahovska, and G. Em Karniadakis, Continuum-and particle-based modeling of shapes and dynamics of red blood cells in health and disease, Soft Matter **9**, 28 (2013).
[34] T. Biben, A. Farutin, and C. Misbah, Three-dimensional vesicles under shear flow: Numerical study of dynamics and phase diagram, Phys. Rev. E **83**, 031921 (2011).
[35] O.-Y. Zhong-can and W. Helfrich, Bending energy of vesicle membranes: General expressions for the first, second, and third variation of the shape energy and applications to spheres and cylinders, Phys. Rev. A **39**, 5280 (1989).
[36] A. Guckenberger and S. Gekle, Theory and algorithms to compute Helfrich bending forces: A review, J. Phys. Condens. Matter **29**, 203001 (2017).
[37] C. Pozrikidis, *Boundary Integral and Singularity Methods for Linearized Viscous Flow* (Cambridge University Press, Cambridge, 1992).
[38] A. Nait Ouhra, A. Farutin, O. Aouane, H. Ez-Zahraouy, A. Benyoussef, and C. Misbah, Shear thinning and shear thickening of a confined suspension of vesicles, Phys. Rev. E **97**, 012404 (2018).
[39] M. Thiébaud and C. Misbah, Rheology of a vesicle suspension with finite concentration: A numerical study, Phys. Rev. E **88**, 062707 (2013).
[40] G. Ghigliotti, T. Biben, and C. Misbah, Rheology of a dilute two-dimensional suspension of vesicles, J. Fluid Mech. **653**, 489 (2010).
[41] A. Guckenberger and S. Gekle, A boundary integral method with volume-changing objects for ultrasound-triggered margination of microbubbles, J. Fluid Mech. **836**, 952 (2018).
[42] A. Daddi-Moussa-Ider, A. Guckenberger, and S. Gekle, Long-lived anomalous thermal diffusion induced by elastic cell membranes on nearby particles, Phy. Rev. E **93**, 012612 (2016).
[43] S. Quint, A. F. Christ, A. Guckenberger, S. Himbert, L. Kaestner, S. Gekle, and C. Wagner, 3D tomography of cells in micro-channels, Appl. Phys. Lett. **111**, 103701 (2017).
[44] A. Farutin, T. Biben, and C. Misbah, 3D numerical simulations of vesicle and inextensible capsule dynamics, J. Comput. Phys. **275**, 539 (2014).
[45] A. Guckenberger, M. P. Schraml, P. G. Chen, M. Leonetti, and S. Gekle, On the bending algorithms for soft objects in flows, Comput. Phys. Commun. **207**, 1 (2016).
[46] D. Saintillan, E. Darve, and E. S. G. Shaqfeh, A smooth particle-mesh Ewald algorithm for Stokes suspension simulations: The sedimentation of fibers, Phys. Fluids **17**, 033301 (2005).
[47] H. Zhao and E. S. G. Shaqfeh, The dynamics of a non-dilute vesicle suspension in a simple shear flow, J. Fluid Mech. **725**, 709 (2013).
[48] A. Rahimian, S. K. Veerapaneni, and G. Biros, Dynamic simulation of locally inextensible vesicles suspended in an arbitrary two-dimensional domain: A boundary integral method, J. Comp. Physics **229**, 6466 (2010).

[49] G. Danker, T. Biben, T. Podgorski, C. Verdier, and C. Misbah, Dynamics and rheology of a dilute suspension of vesicles: Higher-order theory, Phys. Rev. E **76**, 041905 (2007).
[50] C. Misbah, *Complex Dynamics and Morphogenesis* (Springer, Dordrecht, 2017).
[51] A. Farutin, T. Biben, and C. Misbah, Analytical progress in the theory of vesicles under linear flow, Phys. Rev. E **81**, 061904 (2010).
[52] B. Kaoui, A. Farutin, and C. Misbah, Vesicles under simple shear flow: Elucidating the role of relevant control parameters, Phys. Rev. E **80**, 061905 (2009).
[53] V. V. Lebedev, K. S. Turitsyn, and S. S. Vergeles, Dynamics of Nearly Spherical Vesicles in an External Flow, Phys. Rev. Lett. **99**, 218101 (2007).